LA-UR- *09-00185*

Title: | Terahertz metamaterials

Author(s): | Hou-Tong Chen
Abul K. Azad
Antoinette J. Taylor
John F. O'Hara

Intended for: | Proceedings of SPIE

Los Alamos
NATIONAL LABORATORY
——— EST.1943 ———

Form 836 (7/06)

Terahertz metamaterials

Hou-Tong Chen[a], John F. O'Hara[a], Abul K. Azad[a], Willie J. Padilla[b], Richard D. Averitt[c], and Antoinette J. Taylor[a]

[a]Los Alamos National Laboratory, MPA-CINT, Los Alamos, NM 87545, USA;
[b]Department of Physics, Boston College, Chestnut Hill, MA 02467, USA;
[c]Department of Physics, Boston University, Boston, MA 02215, USA

ABSTRACT

In this paper we present our recent developments in terahertz (THz) metamaterials and devices. Planar THz metamaterials and their complementary structures fabricated on suitable substrates have shown electric resonant response, which causes the band-pass or band-stop property in THz transmission and reflection. The operational frequency can be further tuned up to 20% upon photoexcitation of an integrated semiconductor region in the split-ring resonators as the metamaterial elements. On the other hand, the use of semiconductors as metamaterial substrates enables dynamical control of metamaterial resonances through photoexcitation, and reducing the substrate carrier lifetime further enables an ultrafast switching recovery. The metamaterial resonances can also be actively controlled by application of a voltage bias when they are fabricated on semiconductor substrates with appropriate doping concentration and thickness. Using this electrically driven approach, THz modulation depth up to 80% and modulation speed of 2 MHz at room temperature have been demonstrated, which suggests practical THz applications.

Keywords: Terahertz, metamaterials, modulation

1. INTRODUCTION

Terahertz (1 THz = 10^{12} Hz) science and technology have attracted world wide attentions. Many potential applications have been identified due to the unique properties of THz radiation.[1] For example, it can pass easily through regular packaging and clothes, and it is non-ionizing so it is safer than x-rays, therefore THz radiation could be used in security scanning of personnel and luggage. The molecular vibrational frequencies of many common substances and biological materials match the THz regime, so THz radiation is very attractive in molecular identification and sensing, material characterization, spectroscopy, biomedical imaging. Moreover, THz radiation is a candidate for future wireless communication that requires higher speed and more bandwidth. However, despite these attractive applications, the development of THz technology has been relatively slow, mostly due to the lack of natural materials with useful responses in this regime.[2] This is because the THz radiation occupies the part of the electromagnetic spectrum between infrared and microwave waves, where both the electric and photonic responses of materials die out. During the last two decades, THz time-domain spectroscopy (TDS)[1] and THz quantum cascade lasers (QCLs)[3] represent two of the most important developments, but many THz functional devices and components largely do not exist. Therefore, substantial development beyond what has been accomplished to date are essential to enable sustainable THz technology advance.

Metamaterials are a new class of composite artificial materials that acquire their properties from internal subwavelength structure rather than the materials of which they are composed.[4-6] Metamaterials are built from the bottom up, at the unit cell level, to produce independently tailored electric and magnetic responses to the incident electromagnetic waves over a significant portion of the spectrum including the THz regime.[7,8] These designed materials are ideal for the investigation of novel emerging electromagnetic phenomena from RF to near-visible frequency range, including the exotic effects such as negative index of refraction,[5,6] electromagnetic invisibility,[9] and super-resolution.[10,11] The designed and controllable metamaterial resonant response provides an excellent opportunity in solving the material issue associated with the THz gap, and founds the basis for new devices and components that control and manipulate THz waves.

Email: chenht@lanl.gov

In this paper we present our recent progress in the development of THz metamaterials and their application in the implementation of THz devices and components. THz planar metamaterials and their complementary structures have been designed, fabricated and characterized.[12, 13] Both show electric resonant response and THz transmission consistent with the Babinet's principle.[13] Metamaterial resonance frequencies are usually predetermined by their design which is fixed after they are fabricated, However, when natural materials such as semiconductors are incorporated as part of the metamaterial elements, external stimuli such as photoexcitation enable the tuning of resonance frequencies,[14] thereby alleviating the limit of narrowband operation, an inherent result of the metamaterial resonant response. Moreover, the tunability of semiconductor conductivity upon carrier injection or depletion facilitates new opportunity in dynamic or active control of THz metamaterial resonances,[15, 16] which can find applications in ultrafast switching or electrical modulation of THz radiation.[17, 18]

2. COMPLEMENTARY PLANAR TERAHERTZ METAMATERIALS

Suppose we have two complementary free-standing structures which are ideally thin with infinite conductivity. The original structure is illuminated by the normally incident fields ($\mathbf{E}_{0o}$, $\mathbf{H}_{0o}$) and its complement is illuminated by fields ($\mathbf{E}_{0c}$, $\mathbf{H}_{0c}$). Babinet's principle states that if the polarizations are configured in accordance with the dual sources,[19] i.e., $\mathbf{E}_{0o} = Z_0 \mathbf{H}_{0c}$ and $\mathbf{H}_{0o} = -\mathbf{E}_{0c}/Z_0$, where $Z_0 = (\mu_0/\epsilon_0)^{1/2} = 377 \ \Omega$ is the vacuum impedance, then the sum of the transmission fields is equal to the incident fields, or

$$\tilde{t}_o(\omega) + \tilde{t}_c(\omega) = 1, \qquad (1)$$

where $\tilde{t}_o(\omega)$ and $\tilde{t}_c(\omega)$ are the frequency dependent complex transmission coefficients for the original and complementary structures, respectively.

In the THz frequency range it is technically challenging for split-ring resonator (SRR) based metamaterials to fully realize the conditions where Babinet's principle is applicable. We fabricate planar THz metamaterials on suitable substrates such as high resistivity silicon or gallium arsenide (GaAs) wafers. The fabrication is implemented via standard photolithographic methods, followed by metallization and a liftoff process. The metallization includes 10 nm of titanium as the adhesion layer and 200 nm of gold, which is thicker than the skin depth at THz frequencies but is thin enough in the propagation direction. The metamaterial elements shown in Fig. 1 are a series of subwavelength electrical split-ring resonators with symmetrically designed to minimize or eliminate the magnetic response or any electromagneto effects.[12, 20] Both the original metamaterials and their complements (inversed structures) are designed and fabricated to operate at THz frequencies, and are comprised
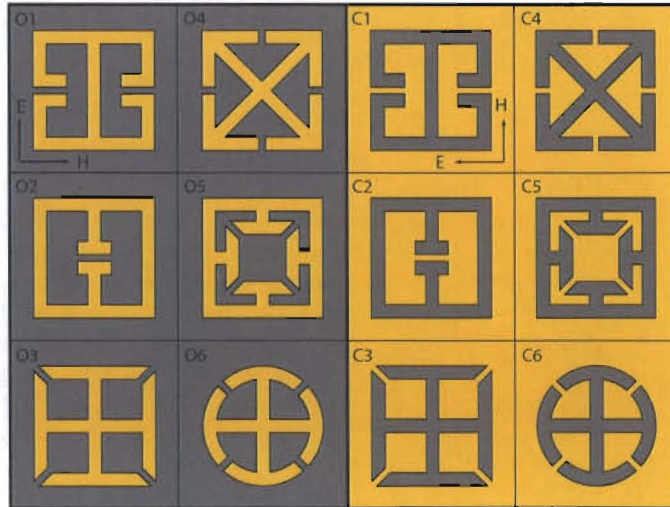

Figure 1. Highly symmetric electric split-ring resonators and their complements as the unit cells for planar THz metamaterials. Colored (light grey) areas indicate gold regions.

of square planar arrays with a lattice parameter of 50 μm. All of these elements have an outer dimension of 36 μm, a line width of 4 μm, and a gap separation of 2 μm.

We use a photoconductive THz-TDS system[21, 22] to characterize the resonant response of metamaterials. The experimental setup includes polyethylene lenses to focus the normally incident linearly polarized THz beam onto a metamaterial sample onto a diameter of about 3 mm, and a second set of polyethylene lenses to focus the transmitted THz beam to a photoconductive receiver. The THz-TDS system is purged with dry air to prevent absorption of THz radiation from water vapor, and all measurements are performed at room temperature. The time-varying electric field of the transmitted impulsive THz radiation $E_s(t)$ is coherently measured in the time domain, and a second measurement $E_r(t)$ is performed through a suitable reference — a bare GaAs substrate of the same thickness. In these measurements, the polarization of the incident THz radiation has been configured as the dual sources for the original and complementary metamaterials. For the structures 1 and 2 in Fig. 1, alternatively it means, under fixed polarization, a sample rotation of 90° around the propagation axis for the complementary metamaterials with respect to their original structures. This rotation is not necessary for the rest of samples due to the $\pi/4$ rotational symmetry. After Fourier transformation of the THz time-domain data, we obtain $\tilde{E}_s(\omega)$ and $\tilde{E}_r(\omega)$ in the frequency domain, which further enables the calculation of the frequency
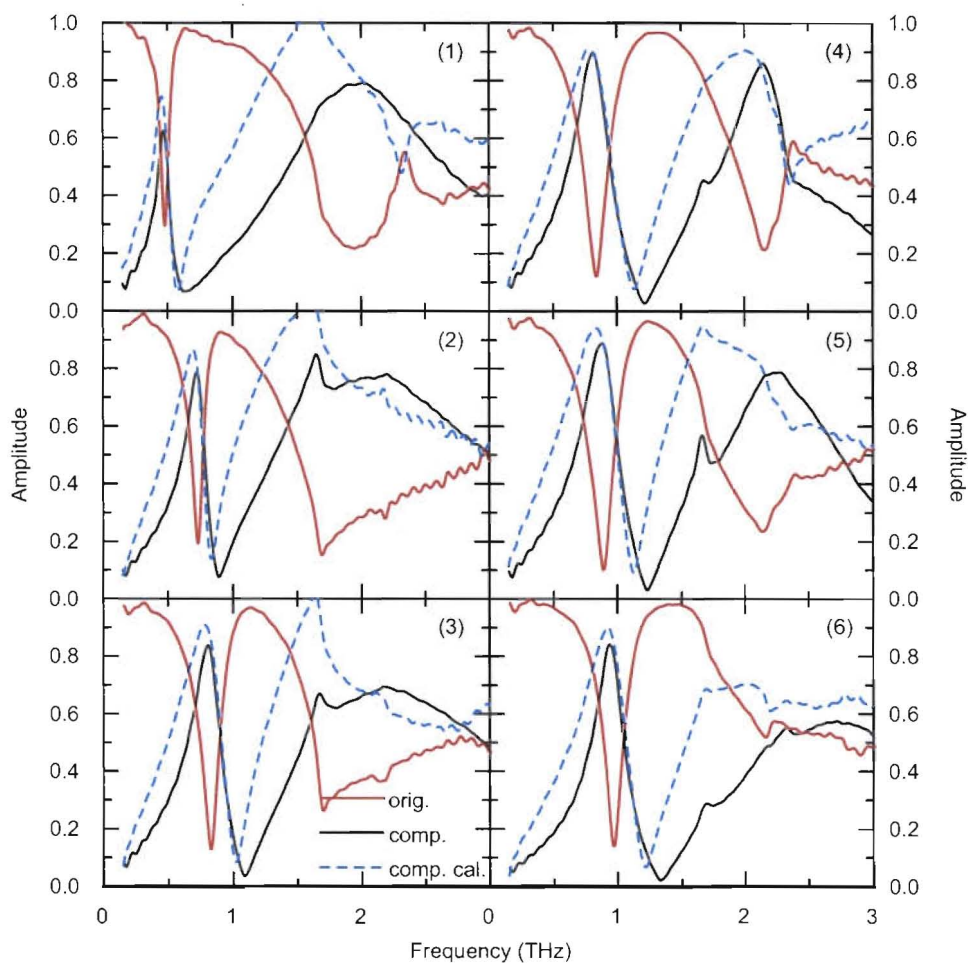

Figure 2. Frequency dependent THz transmission amplitude for the original [red (grey) curves] and complementary (black curves) metamaterials. If the Babinet's principle holds, using the THz transmission data of the original metamaterials, the dashed (blue) curves represent the calculated transmission amplitude for the complementary metamaterials.
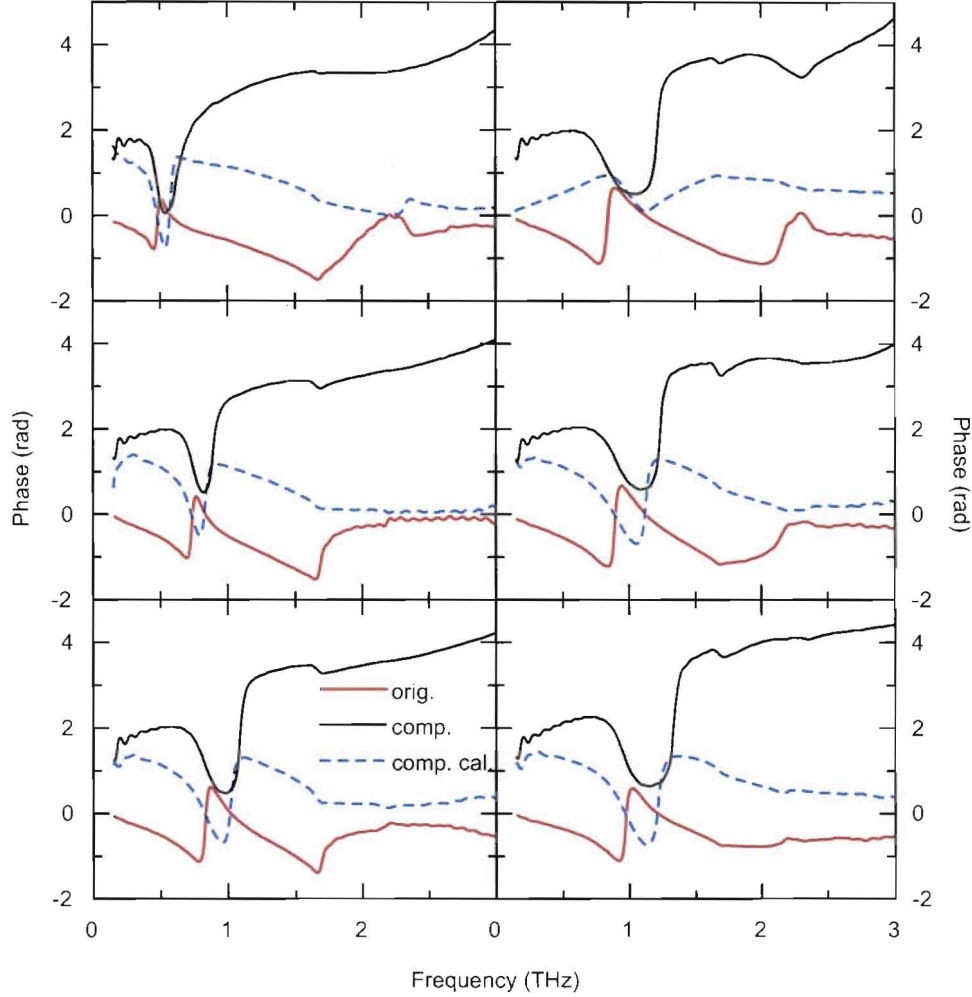
Figure 3. Frequency dependent THz transmission phase introduced by the original [red (grey) curves] and complementary (black curves) metamaterials. If the Babinet's principle holds, using the THz transmission data of the original metamaterials, the dashed (blue) curves represent the calculated transmission phase for the complementary metamaterials.

dependent complex transmission coefficient,

$$\tilde{t}(\omega) = \frac{\tilde{E}_s(\omega)}{\tilde{E}_r(\omega)} = t(\omega)e^{i\phi(\omega)}, \tag{2}$$

where $t(\omega)$ and $\phi(\omega)$ are the frequency dependent transmission amplitude and phase through the metamaterials. This procedure eliminates the substrate effects such as the reflections at the interfaces. With simultaneous amplitude and phase information in the transmission coefficients we are able to obtain the frequency dependent complex dielectric function (there is no magnetic response) assuming appropriate effective thickness of the metamaterials. However, the effective dielectric function does not have significant meaning in our single layer metamaterials in view of potential applications. For this reason, we simply plot the frequency dependent transmission amplitude and phase, as shown in Figs. 2 and 3, respectively.

In all metamaterials we clearly observe two resonances. In the original metamaterials, the lower frequency resonance originates from the capacitive-inductive coupling of counter-circulating currents in the electric split-ring resonators by the incident electric field. In the complementary metamaterials, the resonance results from a similar way of electrically excited circulating currents, i.e., the metal regions are inductive, and the anti-ring regions are capacitive.[12,13] At frequencies below the resonance, the complementary metamaterials also

show cut-off in transmission due to the Drude-like response from the large metal coverage. The resonance in the original metamaterials is represented by the band-stop transmission minimum at frequencies between 0.5 THz and 1.0 THz with $t(\omega)$ values as low as 10%. The complementary metamaterials, on the other hand, show band-pass transmission property with transmission maximum $t(\omega)$ as high as 90% at the same frequencies as in the original metamaterials. Therefore these metamaterials can serve as either band-stop or band-pass far-infrared filters, in which the frequencies can be engineered by scaling the structure dimensions. The higher frequency resonance originates from the electrical excitation of collective dipolar response, in which the resonance frequency also depends on the periodicity of the structures.[23] This is similar to the surface plasma resonances in periodic metal structures. Recently there are arguments of magnetic response in the complementary metamaterials,[24] however, we emphasize that the lower frequency resonances in both the original and complementary metamaterials are purely electric, since it is the incident electric field that drives the surface currents while the in-plane magnetic field has no way to excite such surface currents. Additionally, the counter-circulating currents in each unit cell eliminate any electromagneto response; even if there are magnetic dipoles from the circulating currents, their re-radiation is in the metamaterial plane thus is not able to reach the THz receiver.

From Figs. 2 and 3 it is obvious that the transmission amplitude and phase are interrelated for the original and complementary metamaterials. Suppose Babinet's principle holds, from the transmission data of original metamaterials, we calculate using Eq. (1) the frequency dependent transmission amplitude and phase of the complementary metamaterials, as shown by the dashed curves in Figs. 2 and 3. The complementary metamaterials transmission amplitude spectra are well reproduced as compared to the experimental data, particularly at lower frequencies. The main features of the phase spectra are also reproduced, while the experimental data has additional features, which may result from the different substrate thickness adding the additional frequency dependent propagation phase. This is more significant at higher frequencies as the phase deviation is increasing, affecting the amplitude spectra.

3. ULTRAFAST DYNAMICALLY SWITCHABLE TERAHERTZ METAMATERIALS

The strong resonant response in planar metamaterials forms the basis for many novel THz devices. For many potential applications, it is desirable to use metamaterials with an externally controllable active, dynamical, and/or tunable response. There are many factors that may affect metamaterial resonances. For example, the substrate dielectric constant, together with the structure dimensions, determines the metamaterial resonance frequency. The loss in the metal and substrate, on the other hand, sets the oscillator strength. This motivates us to consider using semiconductors as the metamaterial substrates, in which the conductivity (or loss) can be conveniently modified by external stimuli, e.g., photoexcitation. The photo-induced free charge carriers increase the conductivity on the substrate surface, thereby shorting out the split gaps when circulating currents are excited by the incident electromagnetic fields, and turning off the metamaterial resonance.

In the initial tests we fabricate split-ring resonator array on the intrinsic GaAs substrate using the conventional photolithographic approaches, with the unit cell shown in the inset to Fig. 4 and structure dimensions the same as in the previous section. The metallization consists of 3 μm thick of copper, although such thick metal is not necessary as long as it is more than the skin depth, typically about 50 nm for good metals at THz frequencies. The planar metamaterial is characterized by optical-pump THz-probe[25] measurements, where the femtosecond laser pulses excite the sample, and the dynamic response is probed by measuring the THz transmission in the time domain. In Fig. 4 the metamaterial shows two resonances driven by the electric field of the normally incident THz radiation. The lower frequency resonance results in strong electric field concentration within the split gaps, therefore it is expected that this resonance has strong dependence upon the material properties near the gaps. We investigate the resonant transmission when the metamaterial is under photoexcitation using 50 fs near-infrared laser pulses as a function of the photoexcitation power. In experiments the photoexcitation is 5 ps before the arrival of the THz pulses, which ensures the long lived carrier density has been established.

In Fig. 4 we show the THz transmission amplitude spectra as a function of the photoexcitation power. At a photoexcitation power of 0.5 mW, which corresponds to a fluence of 1 μJ/cm^2 resulting in a photoexcited carrier density of $n \sim 2 \times 10^{16}$ cm^{-3}, the lower frequency resonance is strongly affected, while the higher frequency resonance is less changed. Increasing the photoexcitation power, the lower frequency resonance is continuously damped and at 1 mW it is nearly completely quenched, as reflected by no significant transmission dip. The

THz transmission is switched from 15% to 70% with this low photoexcitation power. At this point the higher frequency resonance also starts to quench, and it nearly disappears at a photoexcitation power of 5 mW. It is reasonable that the switching of the higher frequency resonance requires a higher photoexcitation power due to a lower concentration of electric field at resonance.

The switching off of metamaterial resonances is mainly determined by the photoexcitation of free charge carriers in the GaAs substrate, which could occur very fast when using femtosecond laser pulses. However, the switching recovery is very slow, as the carrier lifetime in the GaAs substrate can be as long as nanoseconds. Obviously, this will limit some potential applications if the ultrafast switching recovery is also highly desired. One solution to this problem is to reduce the carrier lifetime in the substrate, for example, using radiation damaged silicon or low temperature grown GaAs, in which the carrier lifetime can be sub-picosecond. Here we use ErAs/GaAs nanoisland superlattice as the metamaterial substrate, where the carrier lifetime can be conveniently controlled by changing the periodicity of the superlattice.[26] In this particular investigation we design the carrier lifetime of 10 ps, significantly longer than the picosecond duration of the incident THz pulses. The THz transmission is measured using optical-pump THz-probe experiment system with fixed photoexcitation power and as a function of the time delay between the photoexcitation and THz pulses arrival. The transmission amplitude spectra are shown in Fig. 5 for various time delays. With no photoexcitation, where the THz pulse arrives before
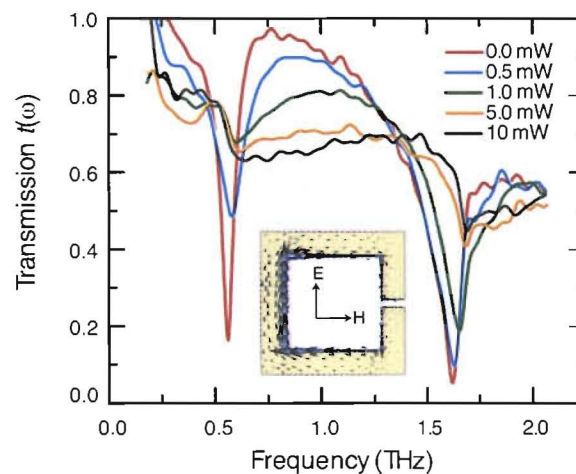

Figure 4. THz transmission amplitude spectra as a function of photoexcitation power of the metamaterial fabricated on intrinsic GaAs substrate. The inset illustrates the unit cell split-ring resonator structure as well as the resonant surface currents at the lower frequency resonance.
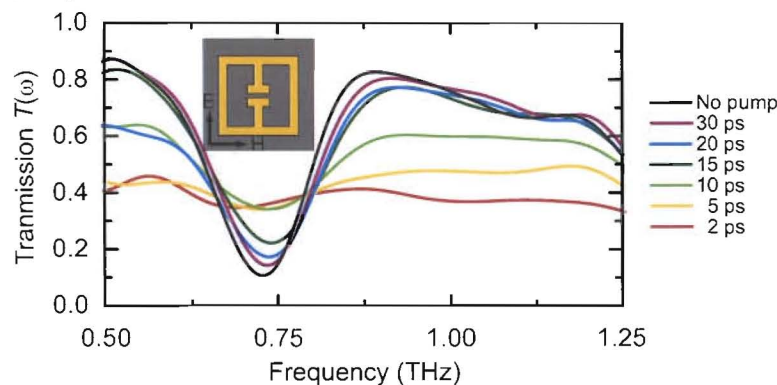

Figure 5. THz transmission intensity spectra of the metamaterial fabricated on ErAs/GaAs nanoisland superlattice substrate with carrier lifetime ~10 ps. The THz transmission is measured as a function of time delay between the photoexcitation and THz pulses arrival.

the photoexcitation pulse, the transmission dip with a small minimum indicates a strong resonance. Under photoexcitation after a short time delay, the carrier density is still high since the carriers do not have enough time to recombine yet, and therefore the metamaterial resonance is switched off within less than 2 ps, as suggested by the flat transmission spectrum at 2 ps time delay. When the time delay increases, the photoexcited charge carriers gradually recombine and the conductivity decreases, thereby the resonance is gradually reestablished, as indicated by the appearance of the transmission dip and the decreasing transmission minimum. Ultimately, the resonance is near fully recovered at about 20 ps time delay. Through this approach, i.e., photoexcitation of the metamaterial substrate with a designed carrier lifetime, we realize both ultrafast switching off and switching recovery of metamaterial resonances, and thus such metamaterials can be used as ultrafast THz devices, e.g., all optical switches and modulators.

4. FREQUENCY TUNABLE TERAHERTZ METAMATERIALS

The frequency of metamaterial resonance is usually predetermined during the design and it is fixed once the metamaterial is fabricated. The resonant nature enhances the interaction between THz radiation and metamaterials, but also causes strong dispersion as well as narrow band operation, which may limit many applications where broadband frequency coverage is necessary. Therefore, frequency agile metamaterials are highly desired, for instance, as tunable far-infrared filters . If we consider the resonance frequency $\omega \sim (LC)^{-1/2}$ where L is the loop inductance and C is the gap capacitance, there are two possible approaches to accomplish the frequency tunability: 1) tuning the substrate dielectric constant ϵ_{sub} since $C \propto \epsilon_{sub}$; 2) tuning the physical geometry of the metamaterial structure. In the first approach, the substrate dielectric constant could be actively tuned by applications of heat, electric or magnetic field,[27] etc., for example, using ferroelectric materials. In this section, we demonstrate the second approach of frequency tunable THz metamaterials, in which the semiconductor material becomes an integrable part of the metamaterial elements.[14] The effective geometry of the metamaterial elements is then dependent on the conductivity of the semiconductor regions, which can be tuned over many scales upon photoexcitation of free charge carriers. This is significantly different from the approaches in the previous section, where semiconductors are used as the substrates and the photoexcitation can only switch the resonance strength but is unable to tune the resonance frequency.

The frequency tunable THz metamaterial sample is shown by the scanning electron microscopy graphs in Fig. 6. The fabrication starts with a silicon-on-sapphire (SOS) wafer with (100) silicon layer of 600 nm thick and resistivity greater than 100 Ω-cm. The metal electric split-ring resonator array is first patterned using the standard photolithographic methods, followed by metallization of 10 nm of titanium and 200 nm of gold, and then a lift-off process. The metal stripes that have the split gaps lay along the primary flat orientation
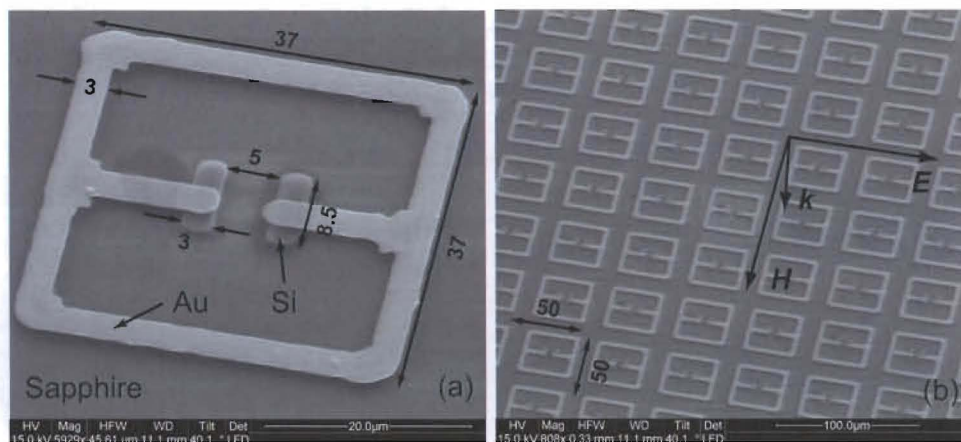

Figure 6. Scanning electron microscopy images of the frequency tunable THz planar metamaterial. (a) An individual unit cell and (b) a square array. All dimensions are shown in μm, and the silicon and gold regions are indicated. The polarization of the normally incident, linearly polarized THz radiation is also indicated.
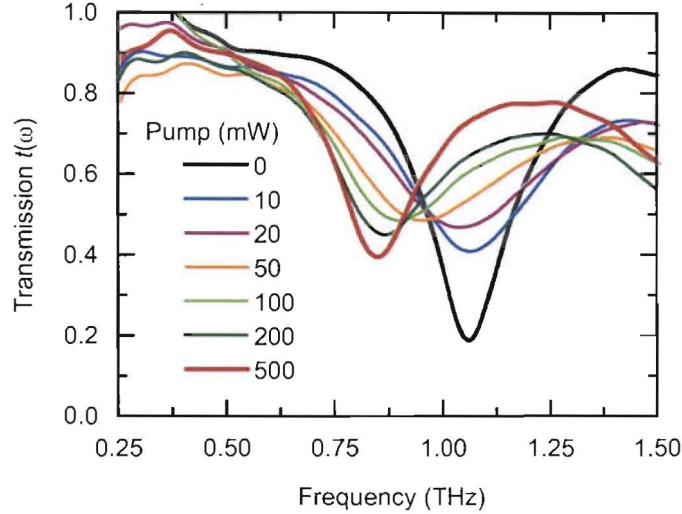
Figure 7. THz transmission amplitude spectra of the frequency tunable THz metamaterial as a function of the photoexcitation power.

of the wafer, that is, 45° counterclockwise from the projection of the C-axis on the R-plane. Next, photoresist pattens are defined at the regions where we want the silicon to be the integrable part of the metamaterial. The photoresist and metal (electric split-ring resonators) serve as the mask during the reactive ion etching (RIE), by which in the unprotected regions the unwanted silicon is removed. In this way, we obtain the sample as shown in Fig. 6, where the silicon regions form the additional capacitive plates when they are highly conducting by photoexcitation.

The fabricated frequency tunable metamaterial sample is characterized by optical-pump THz-probe measurements, in which the photoexcitation is 10 ps before the arrival of THz pulses. The transmitted THz pulses are measured in the time domain for various photoexcitation power, which determines the carrier density or the silicon conductivity. The experimental results are shown in Fig. 7. The transmitted THz electric field amplitude spectrum under no photoexcitation shows a strong resonance as suggested by the transmission minimum of $t(\omega) = 19\%$ at 1.06 THz whereas off-resonance transmission is 90%. At lower photoexcitation power (≤ 20 mW) the resonance initially weakens and broadens, showing little shift in frequency. This is because the silicon conductivity is still too low to affect the resonance frequency — the low conductivity only contributes to the loss and damps the resonance strength. Increasing the photoexcitation power (20–100 mW) the silicon conductivity increases as well, and it starts to shift the frequency of the resonance. At this point, the loss is still high as evidenced by the high transmission minimum of 49%. Upon further increasing the photoexcitation power beyond 100 mW causes continued shifting to lower frequencies and also re-establishes the resonance strength and narrows the linewidth. At a photoexcitation power of 500 mW (a fluence of 0.5 mJ cm^{-2} or a carrier density of $\sim 2.5 \times 10^{18}$ cm^{-3}), we recover the resonance strength by achieving minimum value of $t(\omega) = 40\%$ at 0.85 THz. This represents a frequency tuning range of 20% for this first generation metamaterial device. Additionally, we perform finite-element numerical simulations by using the approximated silicon conductivity from the photoexcitation, and the results are in excellent agreement with the experimental measurements. It is expected that semiconductor materials can also be a part of the loop within the split-ring resonators, and the tuning of conductivity will enable a change of loop size, therefore tuning the resonance frequency as well. This effect has also been verified by numerical simulations.[14]

5. ACTIVELY TERAHERTZ METAMATERIAL DEVICES

Dynamically switchable and frequency tunable metamaterials typically utilize photoexcitation from an amplified femtosecond laser pulses, which is not always available. This is certainly a major drawback. It will be more convenient and suitable for practical applications if we can electrically switch or tune the metamaterial resonances
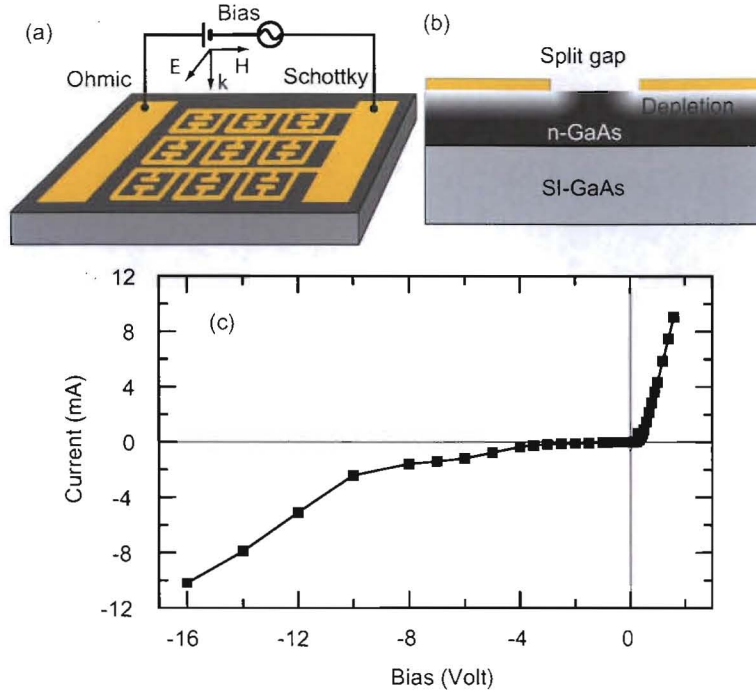
Figure 8. (a)Schematic design of an active THz metamaterial device. (b) The metal metamaterial layer serves as the Schottky gate, and the depletion zone therefore the substrate conductivity, particularly near the split gaps, can be controlled through application of a reverse voltage bias between the gate and substrate. (c) I-V curve for the fabricated device, which shows typical Schottky diode characteristics.

simply by application of a voltage bias. In this section we introduce active THz metamaterial devices[16] fabricated on doped semiconductor substrates, which enable electrical control of the metamaterial resonances, and therefore the switching/modulation of the transmitted THz radiation, upon application of dc or ac voltage bias. This is accomplished through the depletion of charge carriers — electrical control of conductivity of the semiconductor substrate using the metallic metamaterial as the Schottky gate.

The schematic design of the device is shown in Figs. 8(a) and (b). The substrate consists of a 1 μm thick n-type eptaxial GaAs layer with a free electron density of 2×10^{16} cm^{-3} grown on a semi-insulating GaAs wafer. An ohmic contact is first fabricated by e-beam deposition of 20 nm of nickel, 20 nm of germanium, and 150 nm of gold in sequence, followed by rapid thermal annealing at 350°C for 1 minute in a nitrogen atmosphere. Metallic electric split-ring resonator array is then fabricated using standard photolithographic methods to form a square array and connected via metal wires. The metallization consists of 10 nm of titanium and 200 nm of gold. The metallic electric split-ring resonator array and the semiconductor substrate form a Schottky diode structure, as shown in Fig. 8(b), where the depletion zone, particularly near the split gaps, can be actively tuned through application of a reverse voltage bias. The current-voltage relation shown in Fig. 8(c) indicates a typical Schottky behavior.

THz-TDS is used to characterize the performance of the metamaterial device at room temperature. The THz transmission is measured as a function of the reverse bias voltage, and the experimental results plotted in intensity are shown in Fig. 9. Without an applied gate bias, the device is expected to show no or very weak resonant response because of the conducting substrate, which shorts out the capacitive split gaps and no significant resonance can be established. An increasing reverse bias voltage depletes the free charge carriers from the metallic Schottky gate particularly near the split gaps, which reduces the substrate conductivity and restores the resonance strength. As in Fig. 9 the resonances in the transmission spectra narrow and the transmission minimum decreases with increasing reverse bias voltage. At a reverse gate bias voltage of 16 volts, a 50% relative change of transmission intensity is observed at 0.72 THz, the frequency of the LC resonance. Very recently, it is
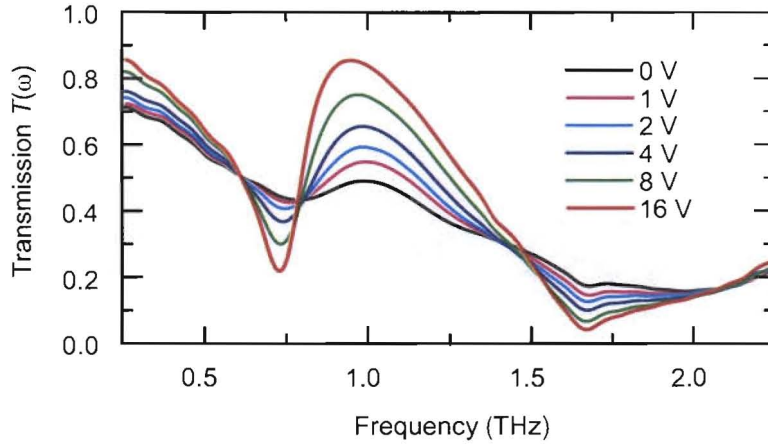
Figure 9. THz transmission intensity spectra as a function of the applied reverse voltage bias.

improved up to 80% with modified structure design. This is more than one order of magnitude improvement over the previous demonstration of electrically-driven THz modulator based on semiconductor quantum structures,[28] making this device a reasonably efficient narrowband THz switch/modulator. We note that the collective dipolar resonance at 1.65 THz is also switched upon the application of voltage bias though its overall transmission is low. This is because the depletion of free charge carriers reduces the overall loss but is not associated with the shorting of the capacitive gaps of the slit-ring resonators.
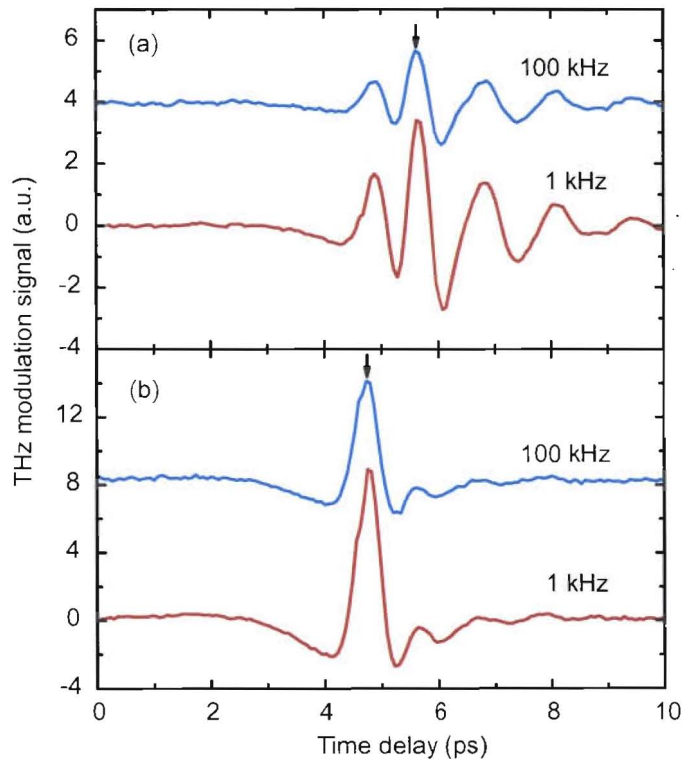

Figure 10. (a) THz-TDS measurements of the modulation (differential) signal at 1 and 100 kHz. (b) THz-TDS measurements by applying square ac voltage to the photoconductive THz emitter at 1 and 100 kHz to shown the system response. The arrows indicate the time positions where we perform the frequency response measurements.

When applying an ac bias voltage to the metamaterial device, it is expected that the transmitted THz radiation will be modulated. We perform THz-TDS measurements of the modulation (differential) signal by application of a square voltage bias alternating between 0 and 12 volts at various modulation frequencies. The results are shown in Fig. 10(a) for 1 and 100 kHz, which suggests the effective modulation of the THz radiation. Because of the large device area (5 mm × 5 mm additional to electrical pads) the device is not expected to operate very fast. Nevertheless, at 100 kHz modulation frequency we still observe effective modulation, roughly half of the modulation signal as compared to 1 kHz. Note that part of this modulation amplitude decrease is due to the THz-TDS system response, i.e., the modulation signal decreases with increasing modulation frequency. This could be verified in Fig. 10(b), where we measured the THz wave forms when the photoconductive THz emitter is modulated at 1 and 100 kHz, as the modulation at 100 kHz is smaller than at 1 kHz. So when we perform measurements to investigate the frequency response of the metamaterial modulation, this THz system response should be eliminated from the experimental data.

In order to obtain the operation speed of the device, we perform measurements of the modulation signal as a function of the modulation frequency. We measure the THz signal with the time position fixed as indicated in Fig. 10(a) while we sweep the modulation frequency. The results is then normalized to the system response, which is obtained from a similar measurement. Fig. 11 reveals the experimental results with roll-off frequency of ~100 kHz. Since our lock-in amplifier can only operate up to 100 kHz, we also load external resistors to lower the role-off frequency by increasing the RC time constant, where C is the device Schottky capacitance, and R is the total resistance including the device forward resistance, output resistance from the function generator, and the external loading resistance. We performed a theoretical estimation of the role-off modulation frequency by calculating the Schottky capacitance, and the results are in good agreement with the measurements.[18] The device modulation speed can be further improved by reducing the active area, eliminating the large electric pads, and using interdigitated ohmic contacts, with which we have demonstrated a modulation speed of 2 MHz.[18]
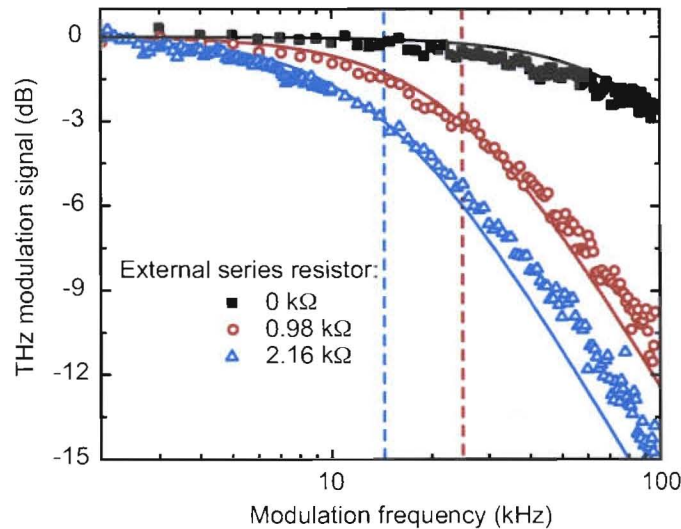

Figure 11. Frequency response of modulation with various external resistance loading.

6. CONCLUSION

In conclusion, we have developed a series of planar metamaterials operating at THz frequencies, which can be easily fabricated by standard micro-fabrication techniques. The band-stop or band-pass transmission properties in the complementary metamaterials is consistent with the Baninet's principle, and can find many applications such as far-infrared filters.[13] The dynamical frequency tunability is achieved by integrating semiconductor materials into the metamaterial building block split-ring resonators, where the photoexcitation tunes the effective capacitive gap. Using semicondutors as the metamaterial substrates, we demonstrate the dynamical switching

of THz metamaterial resonance, and therefore the THz transmission property. The slow switching recovery is overcome by reducing carrier lifetime using materials such as ErAs/GaAs nanoisland superlattice substrate. This approach is expected to be extended to other frequency regimes as well. Finally, the active THz metamaterial devices are able to switch and modulate THz radiation through application of a voltage bias at room temperature with reasonable high modulation depth and speed. These demonstrations elucidates the potential of developing novel THz devices and components for many applications, such as polarization manipulation, anti-reflection, perfect absorption,[29, 30] phase shifting, broadband operation and so on.

ACKNOWLEDGMENTS

REFERENCES

1. D. Mittleman, *Sensing with terahertz radiation*, Springer-Verlag, Berlin, 2003.
2. B. Ferguson and X.-C. Zhang, "Materials for terahertz science and technology," *Nature Mater.* **1**, pp. 26–33, 2002.
3. R. Köhler, A. Tredicucci, F. Beltram, H. E. Beere, E. H. Linfield, A. G. Davies, E. A. Richie, R. C. Lotti, and F. Rossi, "Terahertz semiconductor-heterostructure lasers," *Nature* **417**, pp. 156–159, 2002.
4. D. R. Smith, W. J. Padilla, D. C. Vier, S. C. Nemat-Nasser, and S. Schultz, "Composite medium with simultaneously negative permeability and permittivity," *Phys. Rev. Lett.* **84**, pp. 4184–4187, 2000.
5. R. A. Shelby, D. R. Smith, and S. Schultz, "Experimental verification of a negative index of refraction," *Science* **292**, pp. 77–79, 2001.
6. D. R. Smith, J. B. Pendry, and M. C. K. Wiltshire, "Metamaterials and negative refractive index," *Science* **305**, pp. 788–792, 2004.
7. T. J. Yen, W. J. Padilla, N. Fang, D. C. Vier, D. R. Smith, J. B. Pendry, D. N. Basov, and X. Zhang, "Terahertz magnetic response from artificial materials," *Science* **303**, pp. 1494–1496, 2004.
8. A. K. Azad, J. Dai, and W. Zhang, "Transmission properties of terahertz pulses through subwavelength double split-ring resonators," *Opt. Lett.* **31**, pp. 634–636, 2006.
9. D. Schurig, J. J. Mock, B. J. Justice, S. A. Cummer, J. B. Pendry, A. F. Starr, and D. R. Smith, "Metamaterial electromagnetic cloak at microwave frequencies," *Science* **314**, pp. 977–980, 2006.
10. J. B. Pendry, "Negative refraction makes a perfect lens," *Phys. Rev. Lett.* **85**, pp. 3966–3969, 2000.
11. N. Fang, H. Lee, C. Sun, and X. Zhang, "Sub-diffraction-limited optical imaging with a silver superlens," *Science* **308**, pp. 534–537, 2005.
12. W. J. Padilla, M. T. Aronsson, C. Highstrete, M. Lee, A. J. Taylor, and R. D. Averitt, "Electrically resonant terahertz metamaterials: Theoretical and experimental investigations," *Phys. Rev. B* **75**, p. 041102(R), 2007.
13. H.-T. Chen, J. F. O'Hara, A. J. Taylor, R. D. Averitt, C. Highstrete, M. Lee, and W. J. Padilla, "Complementary planar terahertz metamaterials," *Opt. Express* **15**, pp. 1084–1095, 2007.
14. H.-T. Chen, J. F. O'Hara, A. K. Azad, A. J. Taylor, R. D. Averitt, D. B. Shrekenhamer, and W. J. Padilla, "Experimental demonstration of frequency-agile terahertz metamaterials," *Nature Photon.* **2**, pp. 295–298, 2008.
15. W. J. Padilla, A. J. Taylor, C. Highstrete, M. Lee, and R. D. Averit, "Dynamical electric and magnetic metamaterial response at terahertz frequencies," *Phys. Rev. Lett.* **96**, p. 107401, 2006.
16. H.-T. Chen, W. J. Padilla, J. M. O. Zide, A. C. Gossard, A. J. Taylor, and R. D. Averitt, "Active terahertz metamaterial devices," *Nature* **444**, pp. 597–600, 2006.

17. H.-T. Chen, W. J. Padilla, J. M. O. Zide, S. R. Bank, A. C. Gossard, A. J. Taylor, and R. D. Averitt, "Ultrafast optical switching of terahertz metamaterials fabricated on ErAs/GaAs nanoisland superlattices," *Opt. Lett.* **32**, pp. 1620–1622, 2007.

18. H.-T. Chen, S. Palit, T. Tyler, C. M. Bingham, J. M. O. Zide, J. F. O'Hara, D. R. Smith, A. C. Gossard, R. D. Averitt, W. J. Padilla, N. M. Jokerst, and A. J. Taylor, "Hybrid metamaterials enable fast electrical modulation of freely propagating terahertz waves," *Appl. Phys. Lett.* **93**, p. 091117, 2008.

19. J. A. Kong, *Electromagnetic wave theory*, John Wiley & Sons, New York, 1990 (second edition).

20. D. Schurig, J. J. Mock, and D. R. Smith, "Electric-field-coupled resonators for negative permittivity metamaterials," *Appl. Phys. Lett.* **88**, p. 041109, 2006.

21. D. Grischkowsky, S. Keiding, M. van Exter, and C. Fattinger, "Far-infrared time-domain spectroscopy with terahertz beams of dielectrics and semiconductors," *J. Opt. Soc. Am. B* **7**, pp. 2006–2015, 1990.

22. J. F. O'Hara, J. M. O. Zide, A. C. Gossard, A. J. Taylor, and R. D. Averitt, "Enhanced terahertz detection via eras:gaas nanoisland superlattices," *Appl. Phys. Lett.* **88**, p. 251119, 2006.

23. G. Acuna, S. F. Heucke, F. Kuchler, H.-T. Chen, A. J. Taylor, and R. Kersting, "Surface plasmons in terahertz metamaterials," *Opt. Express* **16**, pp. 18745–18751, 2008.

24. T. H. Hand, J. Gollub, S. Sajuyigbe, D. R. Smith, and S. A. Cummer, "Characterization of complementary electric field coupled resonant surfaces," *Appl. Phys. Lett.* **93**, p. 212504, 2008.

25. R. D. Averitt and A. J. Taylor, "Ultrafast optical and far-infrared quasiparticle dynamics in correlated electron materials," *J. Phys.: Condens. matter.* **14**, pp. R1357–R1390, 2002.

26. C. Kadow, S. B. Fleischer, J. P. Ibbetson, J. E. Bowers, A. C. Gossard, J. W. Dong, and C. J. Palmstrøm, "Self-assembled eras islands in GaAs: Growth and subpicosecond carrier dynamics," *Appl. Phys. Lett.* **75**, pp. 3548–3550, 1999.

27. T. Driscoll, S. Palit, M. M. Qazilbash, M. Brehm, F. Keilmann, B.-G. Chae, S.-J. Yun, H.-T. Kim, S. Y. Cho, N. M. Jokerst, D. R. Smith, and D. N. Basov, "Dynamic tuning of an infrared hybrid-metamaterial resonance using vanadium dioxide," *Appl. Phys. Lett.* **93**, p. 024101, 2008.

28. T. Kleine-Ostmann, P. Dawson, K. Pierz, G. Hein, and M. Koch, "Room-temperature operation of an electrically driven terahertz modulator," *Appl. Phys. Lett.* **84**, pp. 3555–3557, 2004.

29. N. I. Landy, S. Sajuyigbe, J. J. Mock, D. R. Smith, and W. J. Padilla, "Perfect metamaterial absorber," *Phys. Rev. Lett.* **100**, p. 207402, 2008.

30. H. Tao, N. I. Landy, C. M. Bingham, X. Zhang, R. D. Averitt, and W. J. Padilla, "A metamaterial absorber for the terahertz regime: Design, fabrication and characterization," *Opt. Express* **16**, pp. 7181–7188, 2008.